J. Fluid Mech. (1966), *vol.* 24, *part* 1, *pp.* 1–31
Printed in Great Britain

Roughness, bluntness, and angle-of-attack effects on hypersonic boundary-layer transition

By H. T. NAGAMATSU, B. C. GRABER AND R. E. SHEER
General Electric Research Laboratory, Schenectady, New York

(Received 5 January 1965 and in revised form 10 May 1965)

An investigation was conducted in a hypersonic shock tunnel to study the laminar boundary-layer transition on a highly cooled 10° cone of 4 ft. length over the Mach-number range of 8·5 to 10·5 with a stagnation temperature of 1400 °K. The effects on transition of tip surface roughness, tip bluntness, and $\pm 2°$ angle of attack were investigated. With fast-response, thin film surface heat-transfer gauges, it was possible to detect the passage of turbulent bursts which appeared at the beginning of transition. Pitot-tube surveys and schlieren photographs of the boundary layer were obtained to verify the interpretation of the heat-transfer data. It was found that the surface roughness greatly promoted transition in the proper Reynolds-number range. The Reynolds numbers for the beginning and end of transition at the 8·5 Mach-number location were $3{\cdot}8 \times 10^6$–$9{\cdot}6 \times 10^6$ and $2{\cdot}2 \times 10^6$–$4{\cdot}2 \times 10^6$ for the smooth sharp tip and rough sharp tip respectively. The local skin-friction data, determined from the Pitot-tube survey, agreed with the heat-transfer data obtained through the modified Reynolds analogy. The tip-bluntness data showed a strong delay in the beginning of transition for a cone base-to-tip diameter ratio of 20, approximately a 35 % increase in Reynolds number over that of the smooth sharp-tip case. The angle-of-attack data indicated the cross flow to have a strong influence on transition by promoting it on the sheltered side of the cone and delaying it on the windward side.

1. Introduction

Knowledge of the laminar boundary-layer transition at high Mach numbers is needed for the development of advanced nose cones, satellites, and space vehicles. Above a Mach number of 8, no theoretical and only limited experimental information is available. The re-entry nose-cone design engineers are thus faced with extrapolating the lower Mach-number data to the re-entry velocities. This usually results in a conservative design, since it is necessary to use protection against turbulent boundary-layer heating. Transition data in the high Mach-number range would allow a more accurate prediction of the necessary heat protection.

Another application for boundary-layer transition knowledge would be in the design of a space plane operating in the Mach-number range of 5 to 26. The engine inlet ramps for this type of plane would most likely be very long, thus favouring boundary-layer transition, which in turn would produce increased boundary-

layer growth, higher heat-transfer rates, and varying inlet performance. Therefore, theoretical and experimental information on boundary-layer phenomena at high Mach numbers is imperative as more sophisticated concepts are developed for future space vehicles.

The stability of the laminar boundary-layer flows to small disturbances has been investigated by Tollmien (1936), Lees (1947), Lin (1955), Schlichting (1960), and others, for both incompressible and compressible flows. Some theoretical analyses show good agreement with the experimental results up to Mach numbers of about 3, but disagree at the higher Mach numbers. For example, the recent theoretical work of Lees & Reshotko (1962) predicts the experimental data of Laufer & Verbalovich (1960) at Mach numbers of 1·6 and 2·2 very well; but the theory does not agree with the results of Demetriades (1958) at a Mach number of 5·8, where it is an order of magnitude lower in Reynolds number than the experimental data. Therefore, an improved stability theory, which would be applicable to Mach numbers greater than 3, is necessary.

The mechanism for the actual breakdown of the laminar boundary layer is still not completely understood. For incompressible flow, the existence of Tollmien–Schlichting waves, which agree with theory, has been confirmed experimentally by Schubauer & Skramstad (1948). Schubauer & Klebanoff (1955) indicated that the transition consisted of the formation of turbulent spots which grow into completely turbulent flow. The recent work of Klebanoff, Tidstrom & Sargent (1962) indicated that the three-dimensional perturbations dominated the turbulent spot or burst formation. Thus, it is fairly well established that the transition from incompressible laminar flow begins with the formation of turbulent bursts.

For supersonic and hypersonic flows up to a Mach number of 8, Laufer & Verbalovich, Demetriades, and Potter & Whitfield (1962) have shown the existence of Tollmien–Schlichting waves in the laminar boundary layer. Potter & Whitfield used hot-wire anemometers to follow the disturbances in the boundary layer but were unable to detect any particular turbulent-burst action. All three sets of data were obtained in continuous-flow facilities and, as a result, the facility itself could possibly mask the turbulent bursts on the model. If there was turbulent flow on the nozzle wall, this probably introduced enough disturbance into the main flow to obscure the turbulent-burst action on the model in what would appear to be background noise of the instrumentation.

In the firing range, there are negligible disturbances ahead of the model, with the result that turbulent bursts have been observed on slender models at supersonic speeds. Jedlicka, Wilkins & Seiff (1954) fired slender ogive-cylinder models at a Mach number of 3·5 and observed the turbulent bursts followed by a laminar boundary layer similar to that noticed by Schubauer & Klebanoff at subsonic velocities with hot-wire probes. Lyons & Sheetz (1961) and Levensteins (1963) fired 10° cone models in the Naval Ordnance Laboratory pressurized ballistic range at Mach numbers of 3·1 and 3·8 and also noticed the turbulent bursts at the beginning of transition. In both of these cases the schlieren and shadowgraphs showed the turbulent bursts to be accompanied by weak shock waves emanating into the flow about the body. The conclusion is thus reached, based on the

available literature, that transition begins with the appearance of turbulent bursts. Further evidence will be given for this conclusion by the data presented in this report.

Aside from the basic mechanism of transition, there is still the question of the effects of Mach number, surface roughness, bluntness, angle of attack, real gas, etc., on the laminar boundary-layer transition. This report will attempt to contribute some insight into the effects of surface roughness, bluntness, and angle of attack for Mach numbers greater than 8. Sputtered platinum surface heat-transfer gauges were used in place of the hot-wire anemometer to monitor the laminar boundary-layer stability. The response of these gauges is approximately 1 μsec as compared to about 10 μsec for the hot-wire. In an earlier paper, Nagamatsu & Sheer (1964) used the heat gauges to indicate the passage of the turbulent bursts and established their speed by measuring the transit time over successive gauges along the cone surface. It was determined that the burst moved at 0·9 of the free-stream velocity, which makes the disturbance subsonic relative to the free stream. A Pitot-tube survey of the boundary layer was made by Nagamatsu, Graber & Sheer (1965) at various reservoir conditions to verify the existence of the different types of boundary layers: laminar, transition, and turbulent. Schlieren photographs of the boundary layer were also obtained and gave support to the other data. With the various techniques, it was always possible to detect the occurrence of transition.

This is one of a series of papers on a continuing study of laminar boundary-layer transition on a 10° cone at hypersonic Mach numbers. More detailed information on the earlier heat-transfer, schlieren, and Pitot-tube boundary-layer survey results can be found in the last two references.

The symbols used throughout the paper are defined as follows:

Nomenclature

C_f	local skin-friction coefficient
C_h	local heat-transfer coefficient
C_P	specific heat at constant pressure
H_0	free-stream stagnation enthalpy
H_w	model wall enthalpy
I_0	constant current through heat gauge, amps
k	thermal conductivity
M	Mach number
P	pressure
P'_0	free-stream Pitot pressure
P'_{04}	boundary-layer Pitot pressure
q	local heat-transfer rate, B.Th.U./ft.^{2} sec
Re_x	Reynolds number based on cone-surface distance
Re_θ	Reynolds number based on momentum thickness
ΔRe_{tr}	incremental change in the beginning transition Reynolds number
R_0	initial heat gauge resistance prior to run
T	temperature
u	local velocity

y distance measured perpendicular to model wall
α angle of attack
β heat-gauge resistance variation coefficient
δ local boundary-layer thickness
ρ local density
σ Prandtl number

Subscripts

b backing material for heat gauge
i incompressible flow conditions
1 local conditions outside boundary layer
5 nozzle reservoir conditions

2. Experimental equipment and instrumentation

2.1. *Hypersonic shock tunnel*

All of the tests were conducted in a hypersonic shock tunnel with a 24 in. diameter conical nozzle attached to a 103 ft. long, constant-area driven tube. A detailed description of the tunnel and the associated instrumentation was published by Nagamatsu, Geiger & Sheer (1959). Combustion of a stoichiometric mixture of hydrogen and oxygen with an excess of helium was used in the driver to produce the desired shock wave in the driven tube. The shock wave reflects from the nozzle entrance and further increases the pressure and temperature. An aluminium diaphragm at the nozzle entrance permits the evacuation of the dump tank and nozzle to a few microns of mercury to facilitate the flow establishment and minimize the strength of the starting shock waves.

2.2. *Model*

The cone model, 4 ft. in length with a 10° included angle, was made in five pieces with five pressure orifices and six heat gauges. To simplify the investigations of the leading-edge roughness and bluntness, the tips shown in figure 1 (plate 1) were made interchangeable and the various tips will be referred to as designated in the figure. For the sharp tips, the leading-edge diameter was approximately 0·002 in. The first static-pressure measuring location on the model was 2·709 in. from the tip and was constructed with a series of 0·032 in. diameter holes around the circumference connected to a cavity holding the pressure transducer. Other 0·125 in. diameter static-pressure orifices were located at 13·728, 24·730, 35·520 and 46·541 in. from the cone tip with the 35·520 in. location being used for the boundary-layer survey. The heat gauges were located on the opposite side of the cone, 180° from the pressure gauges, at 18·722, 22·757, 26·742, 35·396, 40·377, and 45·380 in. from the cone tip. The surface of the cone had approximately a 50 μin. finish.

2.3. *Instrumentation*

Lead zirconate titinate piezoelectric pressure gauges were used to measure the static pressure on the cone surface and the Pitot-tube pressure throughout the boundary layer. The pressure gauges were dynamically calibrated in an 8 in. calibration shock tube over the pressure range encountered in the test section.

For measuring higher pressures such as the free-stream impact and reflected shock-wave pressures at the entrance to the nozzle, the standard Kistler SLM quartz pressure transducers were used. The output of these gauges is much lower than that for lead zirconate titinate, but they are less sensitive to vibrations and temperature variations. The Kistler gauge used in the free-stream impact probe was dynamically calibrated in the 8 in. tube and the reflected-pressure gauges were calibrated with a dead-weight tester.

A single-pass schlieren system with parabolic mirrors of 6 ft. focal length was used to obtain the photographic records of the shock waves and the viscous layers. To obtain good resolution, a spark of about 0·4 μsec duration was used as the light source.

The surface heat-transfer gauges were made of platinum sputtered on a Pyrex backing to a thickness of approximately 350 Å. To prevent shorting-out of the platinum film during high-temperature tests, a thin evaporated film of silicon dioxide was placed over the platinum to insulate it electrically. This coating did not appreciably affect the gauge response time, which remained about 1–2 μsec. The heat gauges were also dynamically calibrated in the 8 in. calibration shock tube, the gauge characteristics being determined as described by Nagamatsu, Weil & Sheer (1962).

3. Experimental procedures and results

The conditions in the test section of the shock tunnel are determined essentially by the nozzle area ratio and the conditions behind the reflected shock at the entrance to the nozzle. The equilibrium stagnation temperature and pressure behind the reflected shock wave are controlled by the strength of the incident shock wave and the initial temperature and pressure in the driven tube. With a combustion driver it is possible to operate over a wide range of reflected temperatures and pressures.

The pressure, P_5, behind the reflected shock wave was measured with a standard Kistler quartz gauge and the corresponding reflected stagnation temperature, T_5, was calculated using the known shock velocity at the end of the driven tube and the equilibrium thermodynamic data for air from the Mollier diagram by Little (1963). To obtain information regarding the air-expansion process in a hypersonic nozzle, an investigation of the static and impact pressures along the axis of the nozzle was conducted and detailed results were published by Nagamatsu, Workman & Sheer (1961). For the present investigation, the reservoir conditions were chosen such that $T_5 = 1400\,°\text{K}$ while P_5 varied from 450 to 2200 psia. These reservoir pressures were high enough to give near-equilibrium conditions before and after the air was expanded in the nozzle. The reservoir-pressure variation essentially represented a Reynolds-number variation at any given model location.

The test section conditions were determined by using a $\frac{3}{4}$ in. hemisphere tip impact probe. A typical time history of the output of this probe divided by the reflected pressure, P_5, is shown in figure 2. As indicated, the reflected reservoir pressure decreases with time while the P_0'/P_5 ratio remains almost constant over a 2 msec period. When this ratio is converted to Mach number, it is observed

that the test-section Mach number is nearly constant over the corresponding period, which indicates that the real-gas effects are small as stated before. The flow establishment time for the shock tunnel was about 0·7 msec, which explains why figure 2 neglects the first millisecond. Therefore, the effective test time of the facility was 2 msec, which was sufficient for the present investigation.

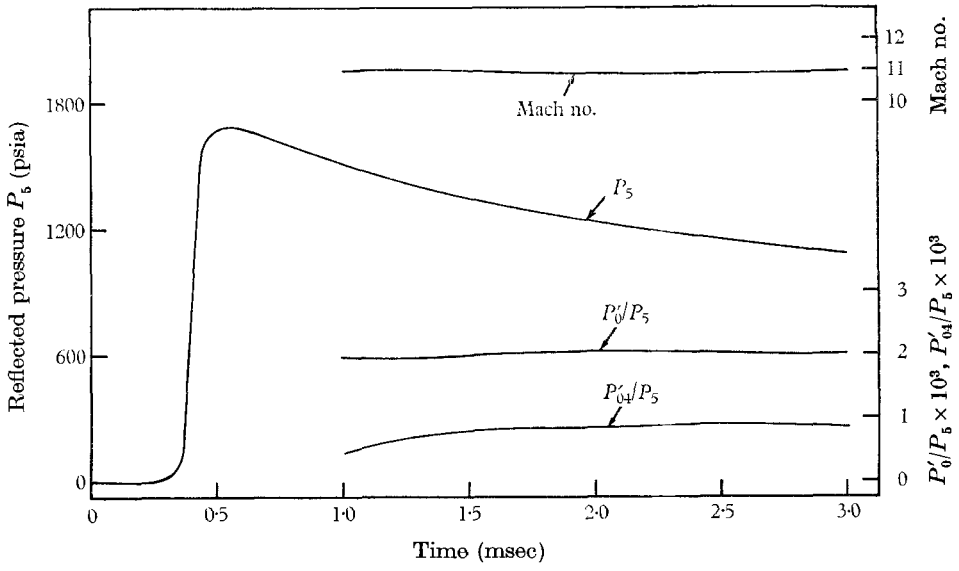

FIGURE 2. Variation of reflected pressure, free-stream impact-pressure ratio, typical boundary-layer impact-pressure ratio and Mach number with time.

Since a conical nozzle, giving source-type flow, was used in the study, the cone model was mounted such that 29 in. of it extended up into the nozzle. In this configuration it was necessary to check the inviscid flow over the model. As indicated in figure 3, the cone surface pressure shows a smooth variation with simply a finite increase over the empty nozzle case due to the change in effective-area ratios. The smooth pressure variation indicated that the model did not introduce any strong disturbances into the basic nozzle flow. It also demonstrates that the flow outside the nozzle was expanding as a free jet. This free-jet expansion was due most likely to the low back pressure, since the dump tank was evacuated to $3\,\mu$ of mercury prior to any run. The low dump-tank pressure also reduced the starting shock strength, which in turn decreased the instrumentation noise.

With the present nozzle-model configuration and source-type flow, a Mach number and pressure gradient existed along the cone surface. The Mach number varied from 8·5 to 10·5 over the six surface heat-transfer gauges. For hypersonic flow expansion, the local temperature, hence speed of sound, decreases so as to counteract the increasing Mach-number gradient and thus the local velocity remains almost constant. This type of variation is not true for subsonic flow, where an increase in Mach number corresponds to a velocity increase. For the present tests, the velocity varied from 5630 to 5744 ft./sec over the six heat

gauges, which gave a 4·29 ft./sec/in. increase. Weil (1951) has calculated the effects of velocity and pressure gradients for compressible flow, based upon the theory of Lin and Lees and found that they are negligible for a free-stream Mach number of 4. As is known, free-stream gradients do affect the stability of incompressible and low supersonic boundary-layer flows. Without a reliable hypersonic

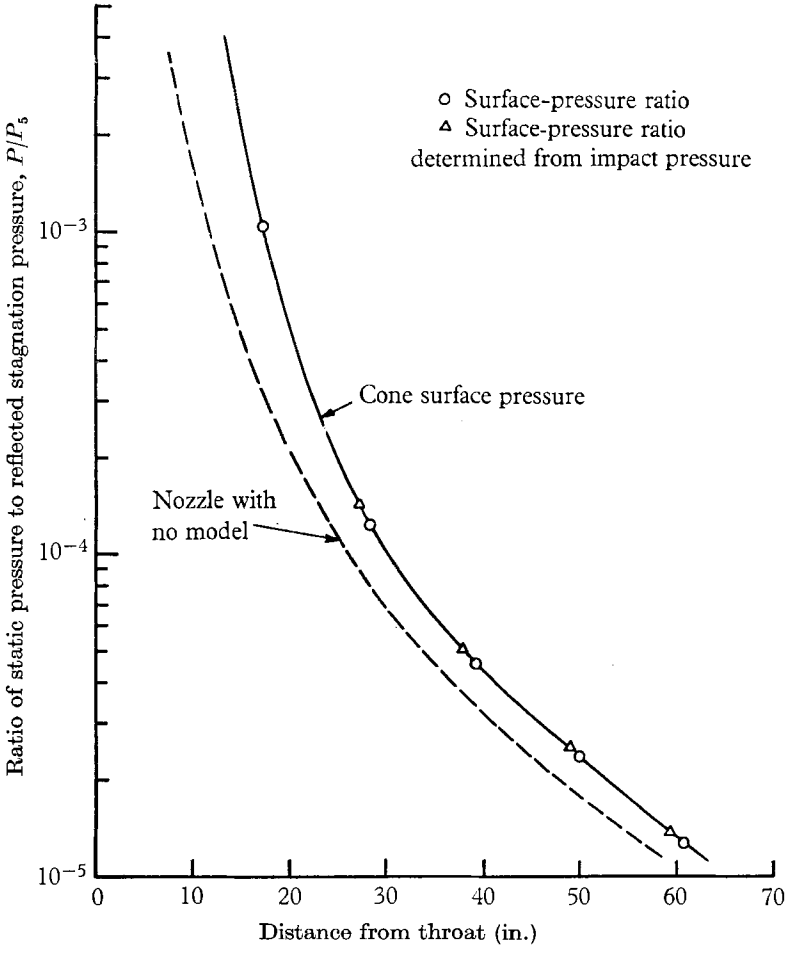

FIGURE 3. Static-pressure distribution for 10° cone in hypersonic nozzle with reflected stagnation pressure, P_5 = 1300 psia, and temperature, T_5 = 1400 °K.

stability theory, it is impossible to predict whether or not these gradients are important at hypersonic Mach numbers. Nevertheless, with the free-stream gradients present, laminar, transition, and fully turbulent flows were obtained and will be discussed in the next section.

The boundary-layer surveys presented were conducted with a circular Pitot-tube probe placed in the number four static-pressure orifice. The inside diameter of the tube was 0·090 in. with a 0·005 in. wall, thus allowing for reasonable response time and limited detrimental probe effects. As to the probe response, figure 2 shows the typical laminar and turbulent P'_{04}/P_5 ratios. After the initial increase

the ratio was constant, indicating steady flow. This was not the picture for the transition flow, as will be pointed out later, where the Pitot tube showed large oscillations.

The angle-of-attack data were obtained by pitching the cone model to plus and minus two degrees. The cone surface-pressure and heat-transfer gauges were kept in a vertical plane with respect to the pitch axis. Also, the two-degree pitch was made in such a way that the cone tip remained on the nozzle axis. Again, the question presented itself as to the effect of this configuration on the basic nozzle flow. As was the case with the zero angle of attack, the measured cone surface-pressure variation remained smooth and changed only in magnitude as the angle of attack changed from plus to minus. This indicated that the configuration did not disturb the basic flow to any greater extent than the zero angle-of-attack configuration.

4. Discussion of results

4.1. *Effects of surface roughness*

(*a*) *Heat transfer*

The output from the heat gauges was converted to local heat-transfer rates by using the equation

$$q(t) = \tfrac{1}{2}\pi^{\frac{1}{2}} \frac{(\rho C_P k)_b^{\frac{1}{2}}}{\beta I_0 R_0} \left\{ \frac{\Delta E(t)}{t^{\frac{1}{2}}} + \frac{1}{\pi} \int_0^t \left(\frac{\lambda}{t}\right)^{\frac{1}{2}} \frac{\Delta E(t) - \Delta E(\lambda)\, d\lambda}{(t-\lambda)^{\frac{3}{2}}} \right\}, \tag{1}$$

where $(\rho C_P k)_b^{\frac{1}{2}}/\beta$ is the gauge characteristic determined in the calibration tube. This equation was integrated on the General Electric 225 computer, which greatly simplified the data reduction. The local heat-transfer rates were converted to heat-transfer coefficients by using the expression

$$C_h = q/\rho_1 u_1 (H_0 - H_w). \tag{2}$$

Initially, the discussion of the heat-transfer data presented for zero angle of attack will be limited to the effects of roughness on the sharp-tip cone configuration. The laminar and turbulent theories presented in figures 5–13 were calculated from the work of Young (1953) and Persh (1955*b*), respectively, using the modified Reynolds analogy of

$$C_h = C_f/2\sigma^{\frac{2}{3}}, \tag{3}$$

where σ is the Prandtl number taken as 0·72 for air. Since both of these theories were flat-plate theories, the transverse curvature correction of $3^{\frac{1}{2}}$ was used in the laminar case. For the tubulent case, no transverse curvature correction was used on the flat-plate theory and, as will be shown, good agreement with the present cone data was obtained.

As indicated earlier, there is an increasing Mach-number gradient, 8·5 to 10·5 over the six heat gauges, and a decreasing pressure gradient along the cone surface. This tends to complicate the discussion of the local surface heat-transfer distribution along the cone surface and as a result only one gauge location will be discussed, so as to limit the variables and simplify the explanation of the various reservoir pressures. The first heat gauge, located 18·722 in. from the cone

tip, will be used as the representative gauge for the discussion of the smooth and rough sharp-tip configurations with the model at zero angle of attack. The Mach number at this gauge is 8·5. It should be understood that any one of the six heat-gauge locations could be used to follow transition as Reynolds number, based on distance along the cone surface, is increased. The discussion would be exactly the same for each gauge location.

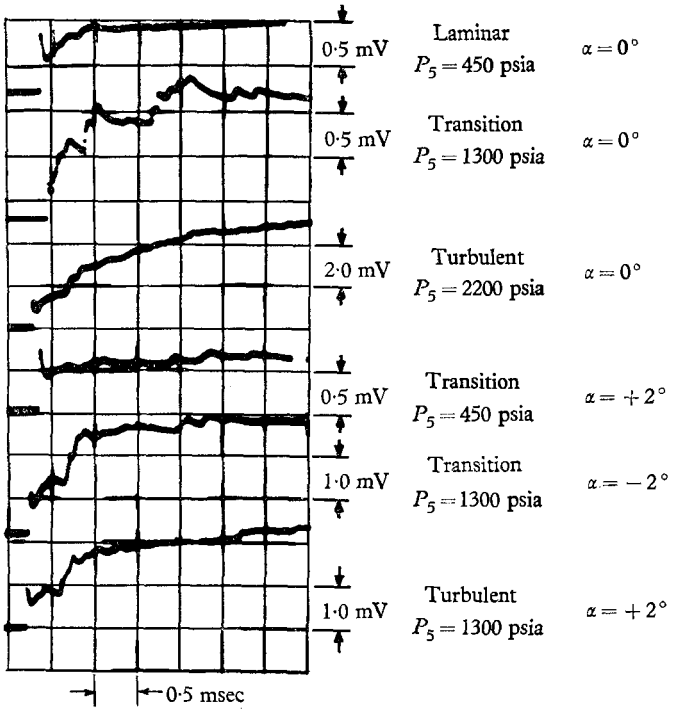

FIGURE 4. Typical heat-transfer traces for smooth sharp tip and varying angles of attack, T_5 = 1400 °K.

Some typical oscilloscope traces of the raw data are shown in figure 4 for zero angle of attack. The laminar boundary-layer flow produced a heat-gauge voltage trace which had a relatively smooth variation and nearly constant output once the basic nozzle flow was established. In contrast, the transition voltage trace showed rather large oscillations which are interpreted as being the passage of turbulent bursts produced in the transition region. For fully turbulent flow, the heat-gauge output returned to a reasonably smooth variation with a superimposed high-frequency oscillation which would be explained by the presence of the eddy motion in a turbulent boundary layer.

Throughout the present study, the reservoir temperature, T_5, was held at approximately 1400 °K while the reservoir pressure, P_5, was varied, which in turn varied the Reynolds number at the first heat-gauge location. The lowest reservoir pressure investigated was P_5 = 450 psia, shown in figure 5. Both the smooth and rough sharp-tip configurations gave a smooth heat-transfer trace with all the data scatter being contained within the symbols. The magnitude of both configurations was about the same and about 30 % above the laminar theory.

The Reynolds number for this reservoir condition was $1{\cdot}95 \times 10^6$ at the first heat gauge. Since the heat-gauge traces were smooth with no noticeable oscillations, the flow was undoubtedly uniform and laminar for both the smooth and rough tips. Tip roughness therefore had no effect on the laminar boundary layer when the Reynolds number was low enough. The agreement of the data with the

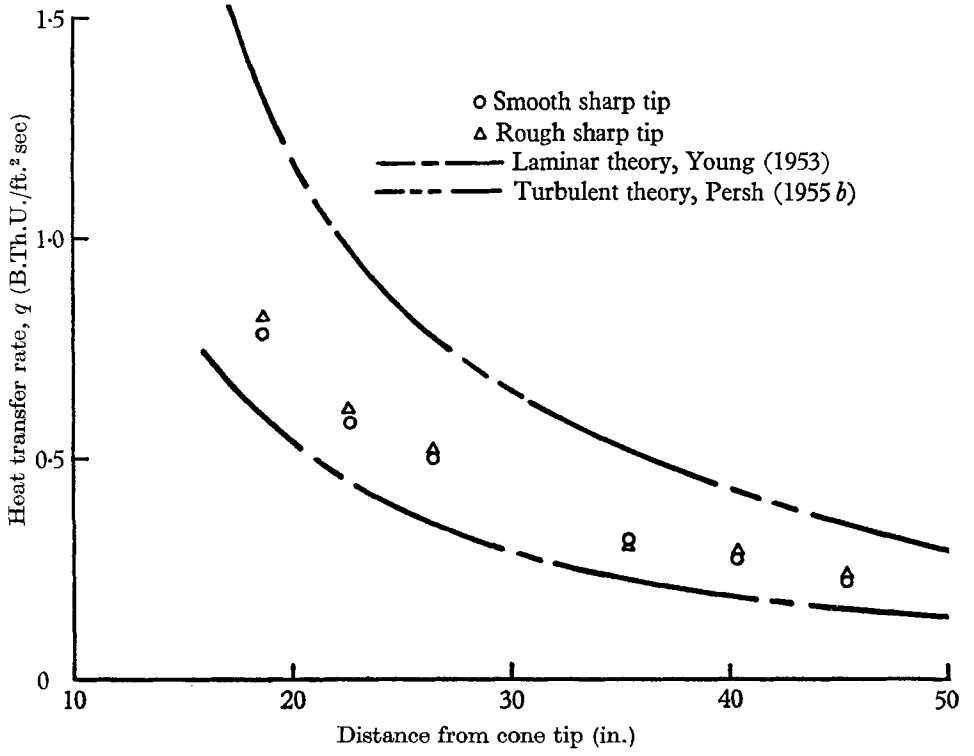

FIGURE 5. Heat-transfer distribution for different cone tips at reservoir pressure, $P_5 = 450$ psia, and temperature, $T_5 = 1400$ °K.

laminar theory is poor, but this could be due to the fact that the pressure gradient is not accounted for in the flat-plate theory. The theoretical and experimental values of the heat transfer differed by 30 % for all laminar cone flow. The existence of the laminar flow was verified by a boundary-layer survey as discussed in the next section.

At the higher reservoir pressure of $P_5 = 585$ psia (figure 6) the Reynolds number at the first heat gauge was $2{\cdot}55 \times 10^6$. Again, the smooth sharp tip gave a smooth uniform trace, indicating laminar flow. It was found after extensive examination that at this reservoir pressure and Reynolds number the first heat gauge for the rough-tip configuration was at the very beginning of transition, where turbulent bursts started appearing over the gauge. Thus, the rough sharp tip, in contrast to the smooth tip, introduced enough disturbances, which were amplified, to cause the formation of turbulent bursts. Increasing the reservoir pressure to 760 psia placed the rough tip well into the transition region, figure 7. The Reynolds number was $3{\cdot}3 \times 10^6$, and with this condition the magnitude of the heat-transfer

with large fluctuations approached the empirical turbulent theory. The transition occurred with the appearance of the turbulent bursts, which showed up on the fast-response heat gauge as a pulse oscillation followed by a smooth trace indicating the return to laminar flow after the passage of the turbulent burst.

The next increase in reservoir pressure to $P_5 = 890$ psia increased the Reynolds number to 4×10^6 at the first heat gauge (figure 8). For this condition, the heat-transfer magnitude for the rough sharp tip compares quite well with the turbulent

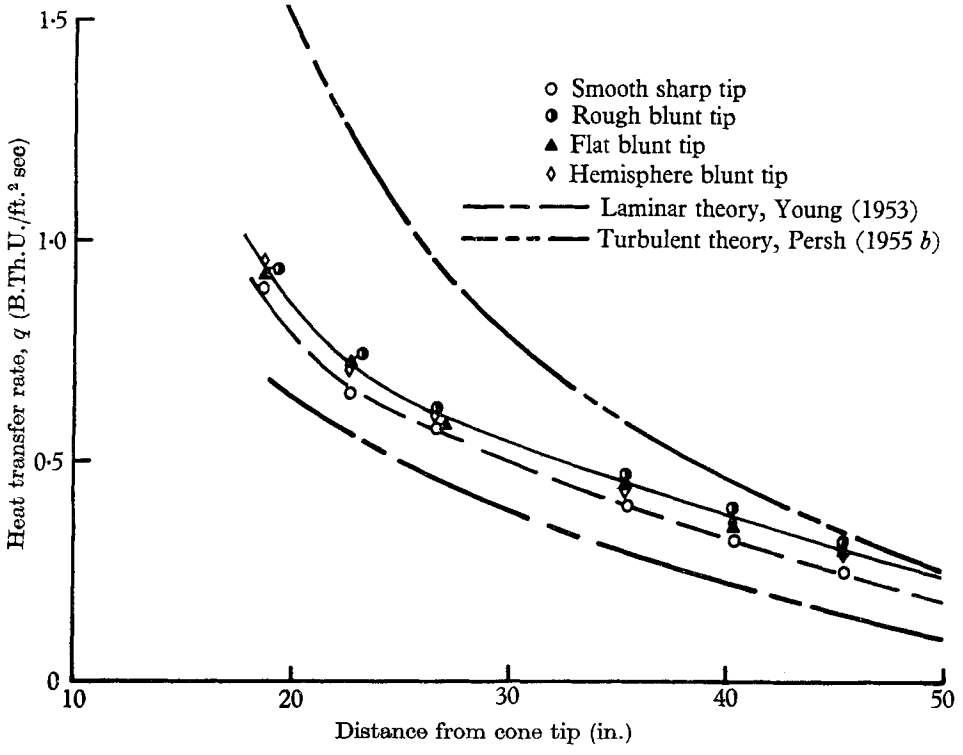

FIGURE 6. Heat-transfer distributions for different cone tips at reservoir pressure, $P_5 = 585$ psia, and temperature, $T_5 = 1400$ °K.

theory, and the heat-gauge trace for the rough tip did not indicate any large oscillations as in the transition case, but only small high-frequency oscillations, which are characteristic of the fully-turbulent boundary layer. On the other hand, the smooth tip shows large oscillations in the value of the heat transfer, the magnitude being less than the rough-tip value and turbulent-theory value, which indicates the smooth-tip boundary layer to be in transition flow. Thus, the rough sharp tip has disturbed the boundary layer sufficiently to force nearly fully turbulent flow at the first heat-transfer gauge, while the smooth tip has only reached transition flow for a Reynolds number of 4×10^6.

From the heat-gauge traces showing transition flow, it was possible to determine the velocity of any turbulent burst as it moved over successive heat gauges along the cone surface. This information showed the burst was moving at approximately 0·9 of the gas velocity outside the boundary layer. This places the

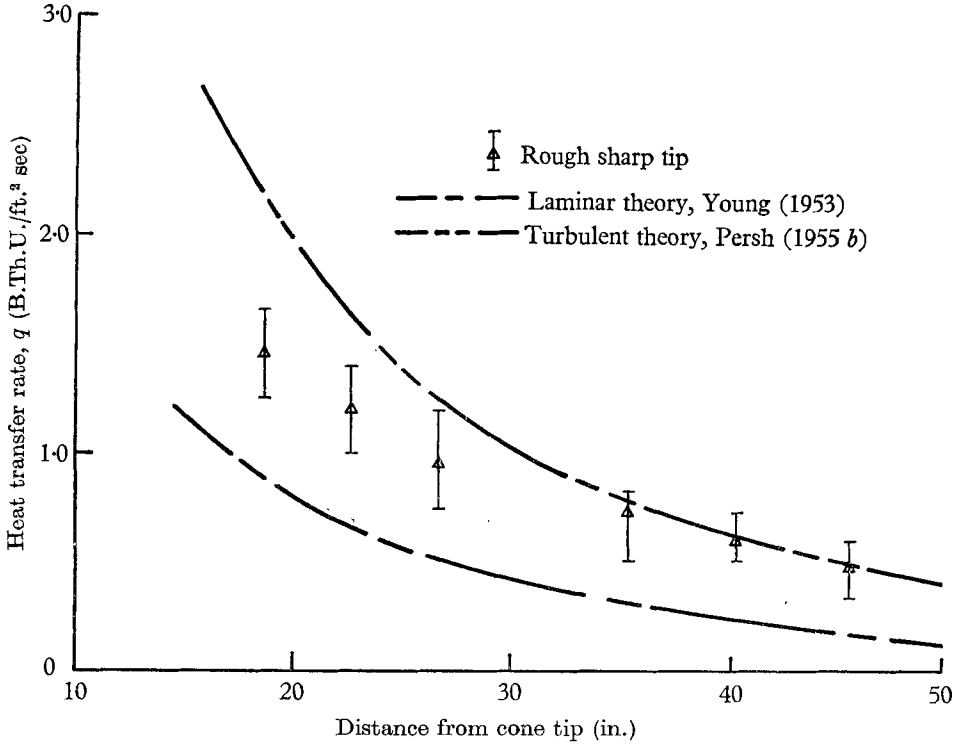

FIGURE 7. Heat-transfer distribution at reservoir pressure, $P_5 = 760$ psia, and temperature, $T_5 = 1400$ °K.

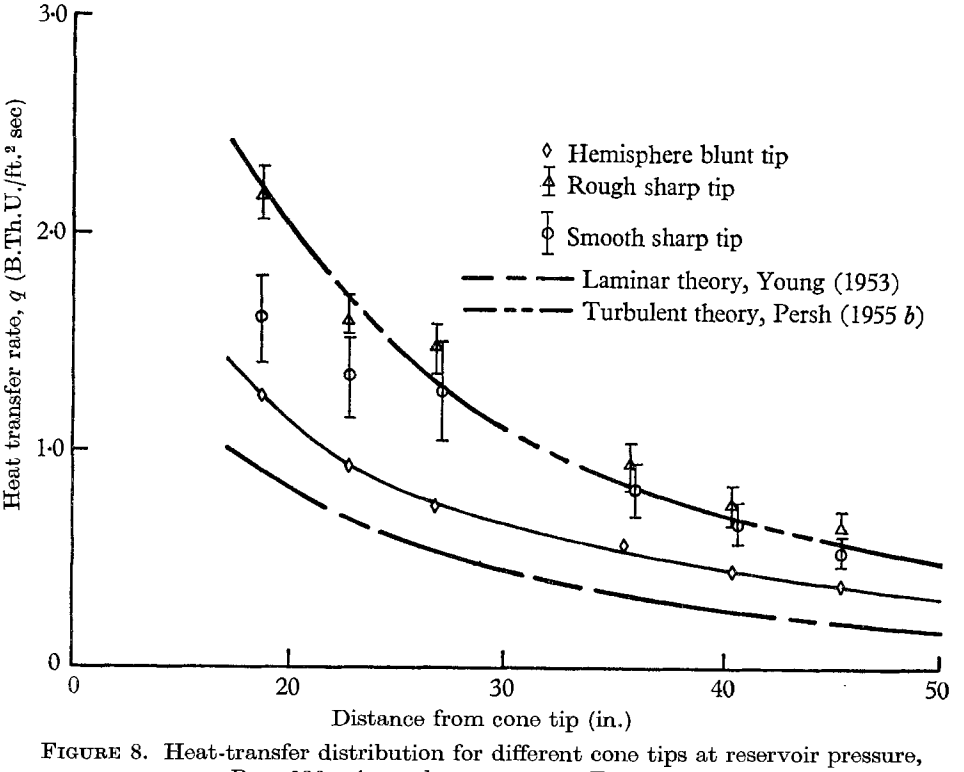

FIGURE 8. Heat-transfer distribution for different cone tips at reservoir pressure, $P_5 = 890$ psia, and temperature, $T_5 = 1400$ °K.

point of maximum oscillation near the outer edge of the boundary layer and establishes that the turbulent-burst velocity was subsonic relative to the free stream. This is significant, since it indicates that the transition process for the present range of Mach numbers is similar to that at lower free-stream Mach numbers, where it has been shown previously that the disturbances are subsonic. This fact helps to justify the assumption, used in all theoretical stability analyses, that supersonic disturbances can be neglected. The stability solution for supersonic disturbances would be extremely difficult to formulate. Even though a good theoretical analysis is not available for the present range of Mach numbers, it is still possible to formulate one using only subsonic disturbances based on the present data.

Using a hot-wire technique, Potter & Whitfield found the critical height, defined as the location of maximum hot-wire output, to be approximately 0·92 of the boundary-layer thickness for a Mach number of 8 and an insulated wall. At subsonic speeds, the critical height is approximately 0·22 of the boundary-layer thickness as observed experimentally by Klebanoff, Tidstrom & Sargent. The present critical height for the cool-wall case seems to agree with Potter & Whitfield's insulated-wall results. Therefore, the large critical-height location might explain why cooling was not entirely effective in stabilizing the laminar boundary layer at hypersonic Mach numbers, since transition was obtained in the present work with a wall-to-stagnation temperature ratio of 0·214.

On increasing the reservoir pressure as shown in figures 9 to 12, the rough sharp tip remained in fully turbulent flow while the smooth sharp tip stayed in transition flow until $P_5 = 2200$ psia. The respective Reynolds numbers at these conditions were $5{\cdot}7 \times 10^6$ at $P_5 = 1300$ psia, $7{\cdot}3 \times 10^6$ at 1800 psia, and $9{\cdot}6 \times 10^6$ at 2200 psia. Hence, the natural transition on the smooth-tip cone required a Reynolds number of $9{\cdot}6 \times 10^6$ to become fully turbulent while the rough tip forced transition and allowed fully turbulent flow to form at a Reynolds number of 4×10^6. Tip roughness, as used in this study, was thus very effective in promoting boundary-layer transition. It might also be noted that, once fully turbulent flow was developed, the local heat-transfer rates agreed quite well with the turbulent theory for both the smooth- and rough-tip configurations. Also, the local heat-transfer oscillations for the smooth- and rough-tip turbulent flows were small compared with those for the transition flow.

The local heat-transfer rates were reduced to coefficient form as previously indicated. When the heat-transfer coefficients were plotted against Reynolds number, based on cone surface distance, the results shown in figure 13 were obtained. This graph deals only with the first heat gauge which was located 18·722 in. from the cone tip, where the local Mach number outside the boundary layer was 8·5. Essentially, figure 13 presents the information discussed in the previous series of figures in summary form. The graph shows the initial flow at low Reynolds number to be laminar with no oscillations. As the Reynolds number increases, the boundary-layer flow moves into the transition region, with large oscillations due to the passage of turbulent bursts over the gauge. When fully turbulent flow is reached for either the rough or smooth tip, the oscillations become high in frequency and small in magnitude. The difference between the

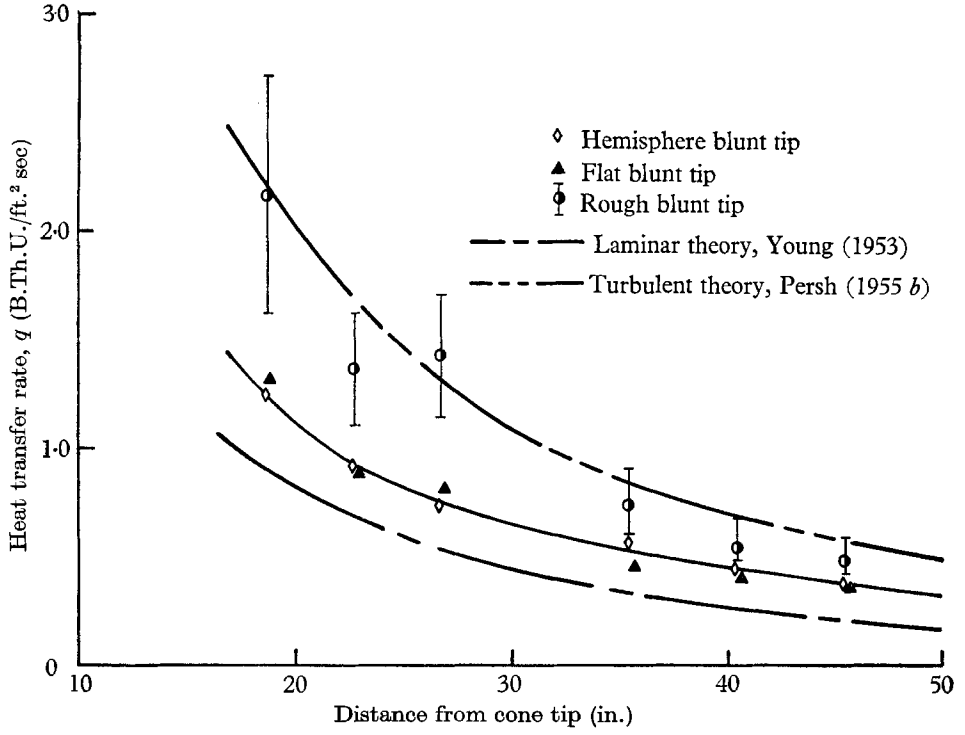

FIGURE 9. Heat-transfer distribution for different cone tips at reservoir pressure, P_5 = 890 psia, and temperature, T_5 = 1400 °K.

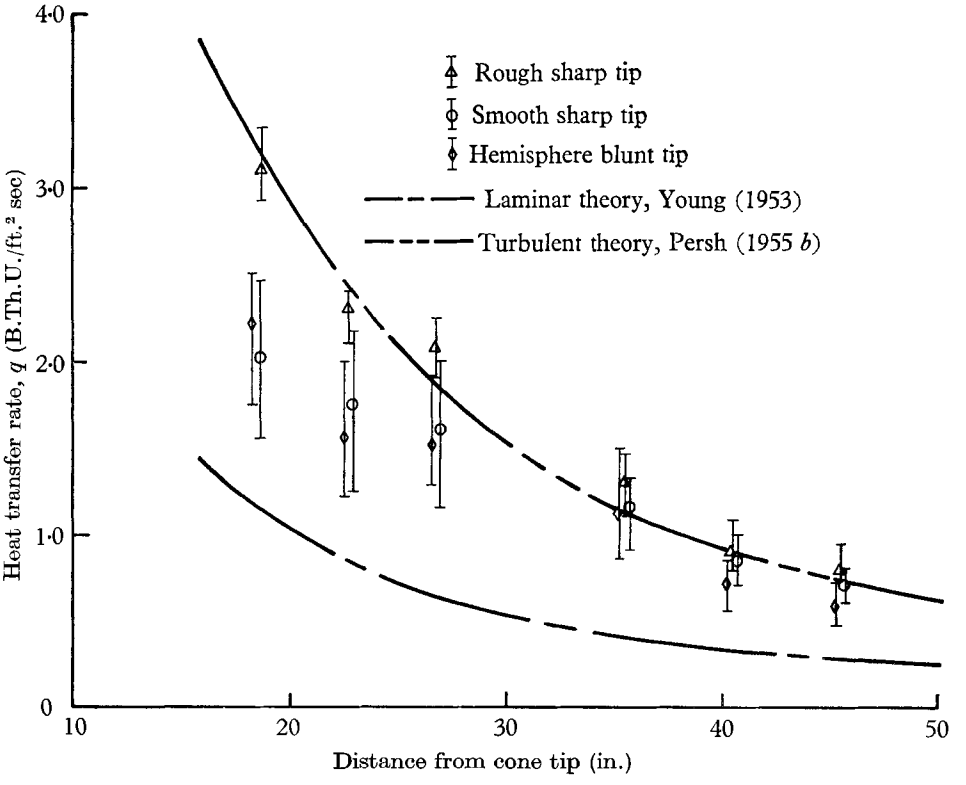

FIGURE 10. Heat-transfer distribution for different cone tips at reservoir pressure, P_5 = 1300 psia, and temperature, T_5 = 1400 °K.

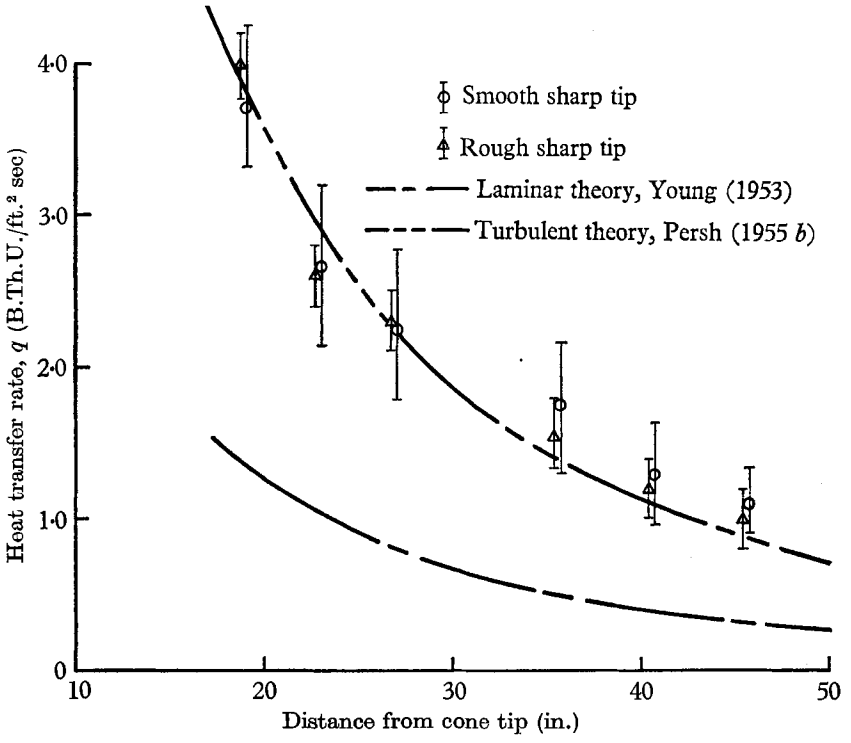

FIGURE 11. Heat-transfer distribution for different cone tips at reservoir pressure, P_5 = 1800 psia, and temperature, T_5 = 1400 °K.

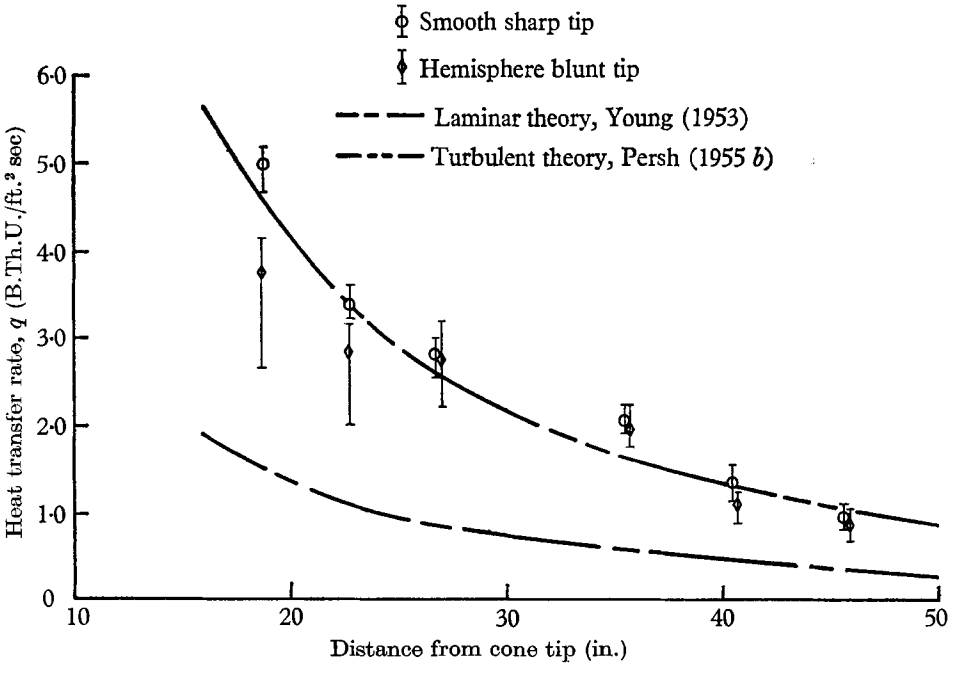

FIGURE 12. Heat-transfer distribution for different cone tips at reservoir pressure, P_5 = 2200 psia, and temperature, T_5 = 1400 °K.

effects of the smooth and rough surfaces on the transition of the boundary layer is evident from this figure. The roughness greatly reduces the length of the transition region compared with the smooth case. Once a high enough Reynolds number is reached, roughness very rapidly causes the boundary-layer flow to become turbulent.

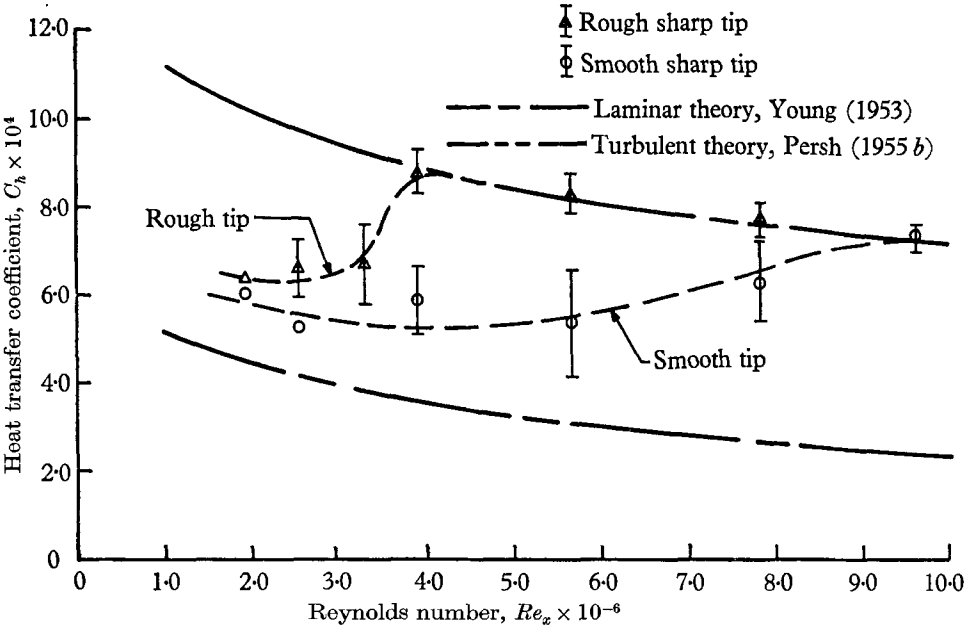

FIGURE 13. Variation of local heat-transfer coefficient with surface Reynolds number for different cone tips at $M = 8{\cdot}5$.

(*b*) *Schlieren photographs*

Schlieren photographs were obtained to support the previous interpretation of the heat-transfer data. A composite series of pictures with the smooth-tip and the rough-tip model are presented in figure 14 (plate 1). To obtain this series of photographs, it was necessary to advance the cone further into the nozzle for each successive picture, since the schlieren windows on the dump tank were at a fixed location just downstream of the nozzle exit. Figure 14 demonstrates visually that boundary-layer transition was actually obtained. For the smooth-tip cone, all the photographs from left to right show a well-defined light to dark boundary which locates the outer edge of the hypersonic laminar boundary layer. A hypersonic laminar boundary layer can be seen with a schlieren system since a steep density gradient exists at the outer edge of the layer. It should be noted that the two right-hand photographs for the smooth tip show some eddies in the light to dark boundary which suggests the presence of turbulent bursts. For comparison, the heat traces for these conditions are presented under the corresponding photographs.

The rough-tip configuration (lower series of photographs in figure 14) indicates the existence of laminar boundary-layer flow in the first three photographs from the left. The next three photographs to the right show the light to dark boundary

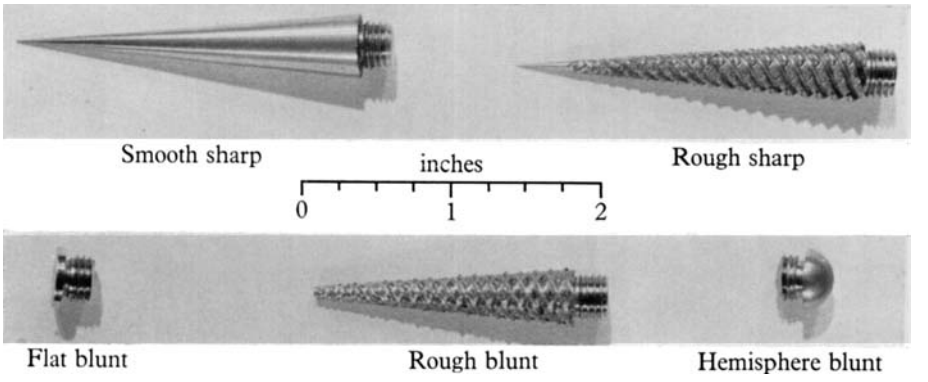

FIGURE 1. Interchangeable tips for 10° cone model.

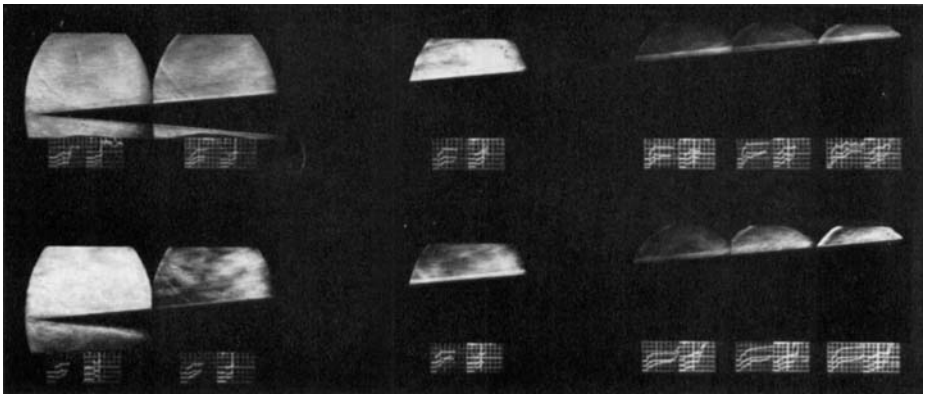

FIGURE 14. Composite schlieren photographs of flow over a 10° cone with smooth sharp (top) and rough sharp (bottom) tips, for reservoir pressure, $P_5 = 1300$ psia, and temperature, $T_5 = 1400$ °K.

fading out into a waffle-type effect due to the turbulent-eddy motion. This is indicative of the turbulent flow, since the turbulent-eddy action would tend to eliminate the sharp density gradients. Hence, the schlieren composite photographs verify the local heat-transfer interpretation and give further evidence of the existence of laminar boundary-layer transition.

(c) *Boundary-layer survey*

A further check on the existence of the various boundary layers was made by probing the layer with a Pitot tube. The initial portion of this work was conducted and reported by Nagamatsu, Graber & Sheer (1965). So far, the discussion has centred on the 8·5 Mach-number location along the cone. In order to have a sufficiently thick boundary layer for probing, it was necessary to move back to the location of Mach number 10, fourth pressure gauge. This will not affect the basic discussion and results because, once a given location along the cone surface becomes fully turbulent, all positions downstream of it are turbulent. Also, as stated earlier, our previous transition discussion would hold true regardless of which heat gauge had been initially selected.

The boundary-layer probing was extended far enough from the wall to measure not only the Pitot pressure within the boundary layer but also the pressure just outside. The results of this investigation are presented in non-dimensional form in figure 15, where the Pitot pressure within the boundary layer is divided by that in the free stream. The laminar and turbulent profiles show very little oscillation while the transition profile indicates large oscillations. It is interesting to note that the Pitot response time was fast enough to follow some of the turbulent-burst oscillations in the transition region. Also, it can be observed that the major oscillations occur towards the outer edge of the boundary layer, which agrees with the heat-transfer data in that the turbulent bursts are moving at 0·9 of the free-stream velocity. The different profiles were obtained at a reservoir temperature of 1400 °K and the following reservoir pressures: smooth-tip laminar $P_5 = 585$ psia; rough-tip turbulent $P_5 = 1300$ psia; smooth-tip turbulent $P_5 = 2200$ psia. In figure 15 the smooth and rough sharp-tip turbulent profiles are exactly the same. Hence, it makes little difference at hypersonic Mach numbers how a boundary layer becomes turbulent, because once it is established it has no past history of any disturbance effects. This same result can be seen in figures 16 to 19, for the other profiles of velocity, density, and temperature.

In order to reduce the boundary-layer impact-pressure data to obtain velocity, temperature, density, and Mach-number profiles, it was necessary to make several assumptions because it was not possible to measure the temperature variation through the boundary layer. The assumptions used were as follows: (1) Ideal-gas flow exists in the test section, $\gamma = 1{\cdot}4$. (2) The wall temperature is constant with $T_w = 300$ °K. (3) The static pressure is constant across the boundary layer. (4) The Prandtl number is equal to unity. (5) The total energy is constant across the boundary layer.

The first assumption is quite justified since at the reservoir temperature of 1400 °K and for the stagnation pressures employed, the real-gas effects were very small with the flow expanding in equilibrium (Nagamatsu, Workman & Sheer).

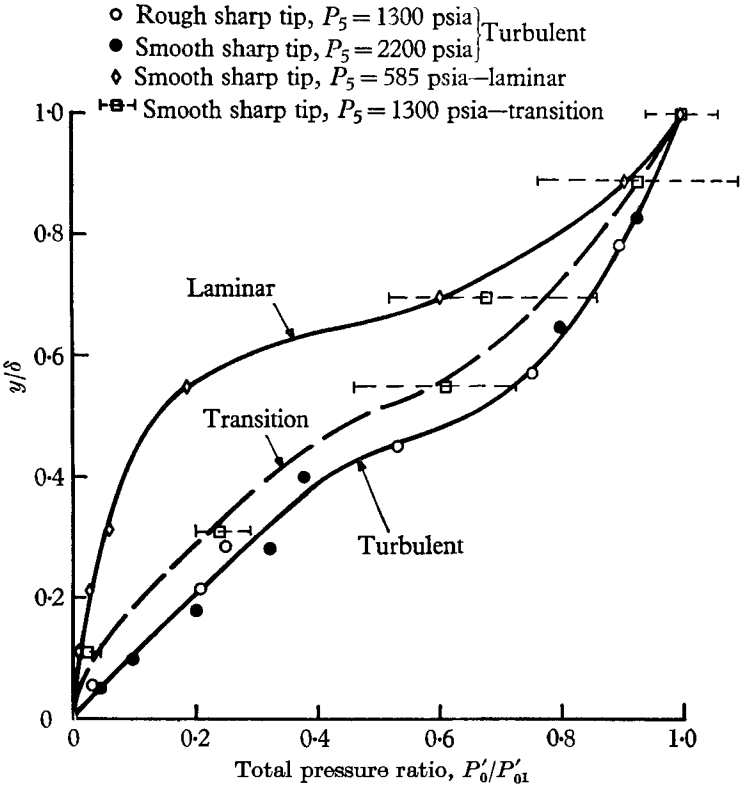

FIGURE 15. Non-dimensional impact-pressure profiles for various types of boundary layers, $T_5 = 1400$ °K, $M_1 \approx 10$.

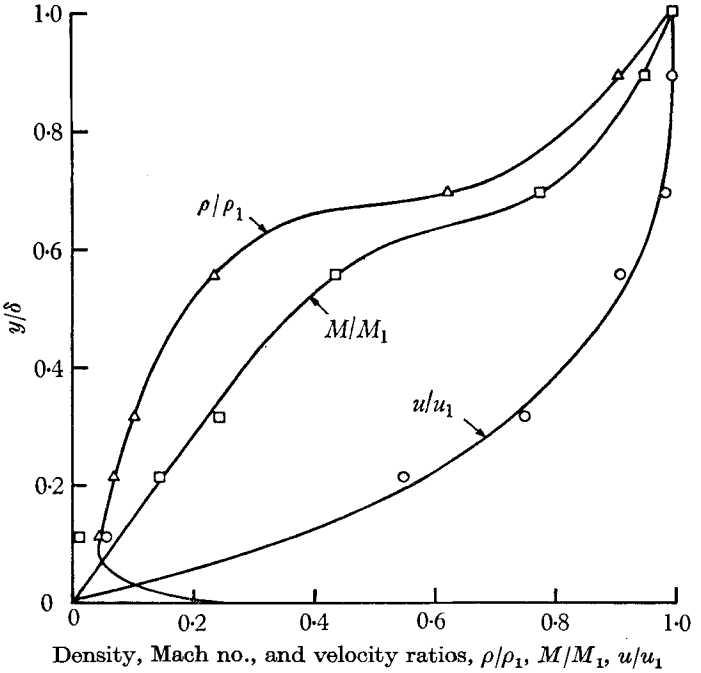

FIGURE 16. Non-dimensional laminar boundary-layer profiles (smooth tip), $P_5 = 585$ psia, $T_5 = 1400$ °K, $M_1 \approx 10$.

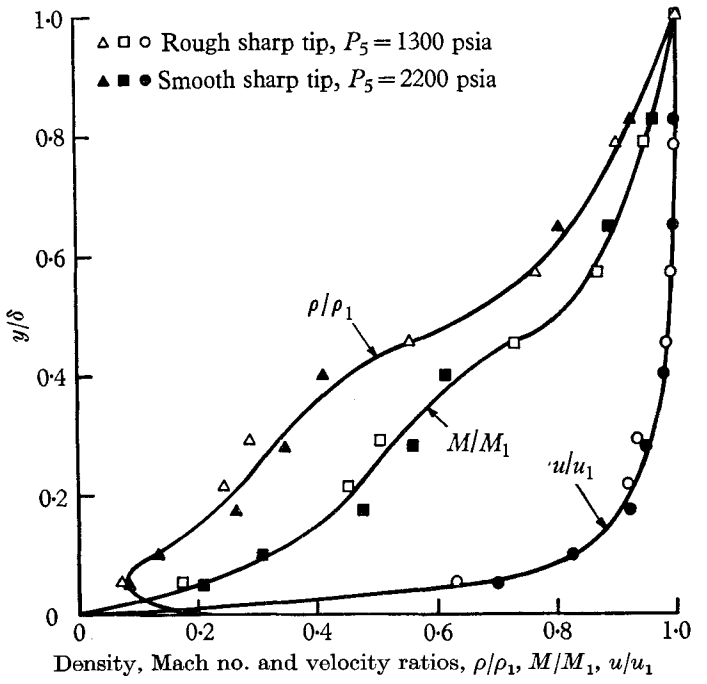

FIGURE 17. Non-dimensional turbulent boundary-layer profiles, $T_5 = 1400$ °K, $M_1 \approx 10$.

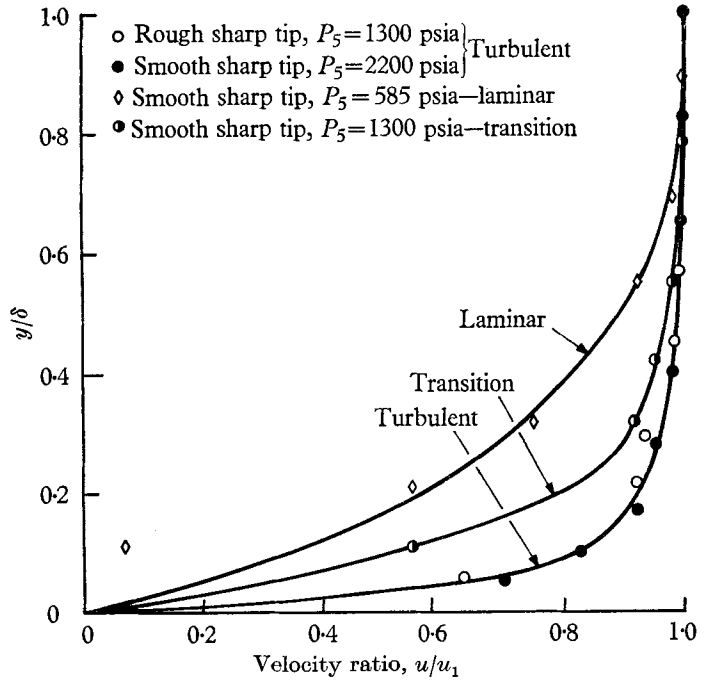

FIGURE 18. Non-dimensional velocity profiles for various types of boundary layers, $T_5 = 1400$ °K, $M_1 \approx 10$.

A short test period of approximately 2·0 msec justifies the second assumption in that there is not enough time for the surface temperature to change significantly. The constant static-pressure assumption is standard for boundary-layer analysis. The last two assumptions are the important ones and have strong implications with respect to the profiles obtained. By assuming a Prandtl number of unity and constant total energy across the boundary layer, one is supposedly dealing with the insulated-wall case of no heat transfer. This is not the case in the present experimental investigation and, as a result, the calculated profiles obtained should be taken as only a first approximation to the true profiles. The actual

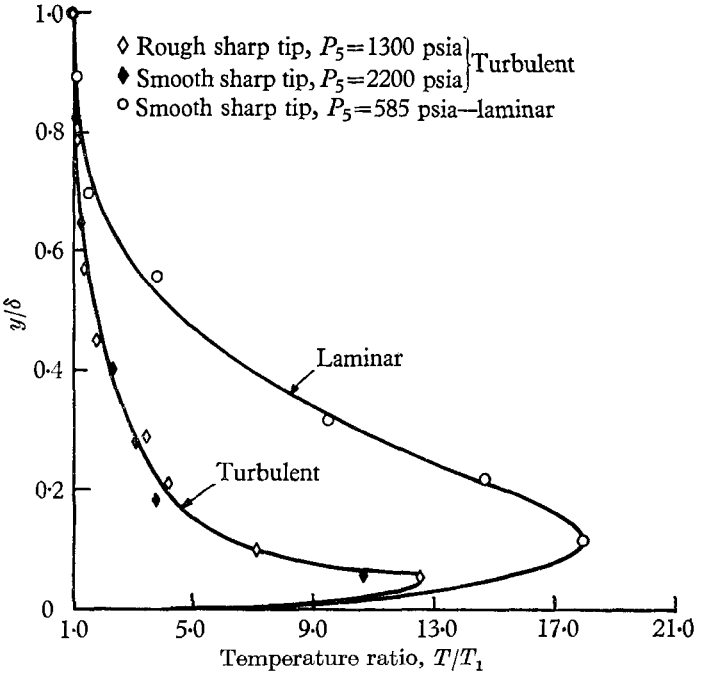

FIGURE 19. Non-dimensional temperature profiles for various types of boundary layers, $T_5 = 1400$ °K, $M_1 \approx 10$.

test situation is one of a cool wall with heat transfer where $T_w/T_0 = 0{\cdot}214$. Nevertheless, the above assumptions should hold fairly well in the outer portion of the boundary layer where the temperature is close to that of the free stream. The validity of these assumptions decreases as one approaches the wall, where the heat-transfer effect becomes important.

By comparing the velocity profiles for the three types of flows (figure 18) a large difference between the laminar, transition, and turbulent cases can be noted. The assumptions used in calculating the profiles make them approximate near the wall, but, by considering the impact-pressure variations presented in figure 15, it is observed that there is a significant difference at $y = \frac{1}{2}\delta$. Using this as a guide, it can be concluded that the difference in the flows existed and was not due entirely to the assumptions employed in the calculations. Also, the assumption of constant enthalpy should be reasonably good for the outer half of the

boundary layer regardless of the wall heat-transfer rates. Comparing the present results with the data of Lobb, Winkler & Persh (1955), where the total temperature through the boundary layer was measured as well as impact pressure, it was estimated that a maximum error of 50 % could exist in the present calculated value of the temperature at the wall. This 50 % error would result in a maximum error of 25 % in the calculated velocity. This error would not account entirely for the observed differences in the profiles, and it would not change the conclusion that laminar, transition, and turbulent flow actually existed at 34·52 in. from the cone tip for the various test conditions. The boundary-layer survey thus further supported the interpretation of surface-roughness effects, and it also demonstrated that the induced turbulent flow is the same as natural turbulent flow.

Using the velocity profiles, the local skin-friction coefficients were determined as accurately as possible. Some judgement must be used in determining the slope of the velocity curve at the wall since it was not possible to make finite measurements right next to the wall. With this in mind, the local skin-friction coefficient was converted to a corresponding heat-transfer coefficient using the modified Reynolds analogy, and it was found that there was reasonable agreement between the boundary-layer profile data and the local heat-transfer data. This agreement helped to verify that the assumptions used in determining the various profiles from the Pitot-tube data had only limited effects on the final profile shapes.

For the turbulent data, the skin-friction coefficient was divided by the incompressible value given by the Karman–Schoenherr equation

$$C_{fi} = 0{\cdot}0568/[\log_{10}(2Re_\theta)]\,[\log_{10}(2Re_\theta) + 0{\cdot}868] \tag{4}$$

and presented in figure 20. In this figure a comparison is made with the experimental data of Lobb, Winkler & Persh; Chapman & Kester (1953); Brinich & Diaconis (1952), and Hill (1956), and with the theories of von Karman (1934); Van Driest (1951), and Wilson (1950). It can be seen that the present data agree reasonably well with the other data and the flat-plate theory of Wilson, which is close to that of Persh (1955*a*). It must be noted that the present data were plotted without any transverse curvature correction. As previously stated, the turbulent heat-transfer values required no transverse curvature correction to agree with the empirical flat-plate theory; thus, it seems possible, as a first approximation, to use the turbulent flat-plate results for small-angle sharp cones at high Mach numbers. Further experimental work is necessary to verify this conclusion.

Another interesting observation is that the momentum Reynolds number, Re_θ, for fully turbulent flow decreases as the Mach number increases. At supersonic Mach numbers, Coles (1954) found that $Re_\theta = 2000$ was sufficient for a turbulent boundary layer, while Hill, at a Mach number of about 9, found that turbulent flow could exist down to $Re_\theta = 1500$. The present work places the turbulent Re_θ value at approximately 1000.

Up to this point, only the effects of surface roughness on the sharp-cone configuration have been discussed. It has been shown that turbulent flow was

obtained and that the surface roughness had a large effect in promoting turbulent boundary-layer flow. Only one heat gauge and Mach-number location along the cone was used in the heat-transfer discussion. Nevertheless, any gauge or Mach-

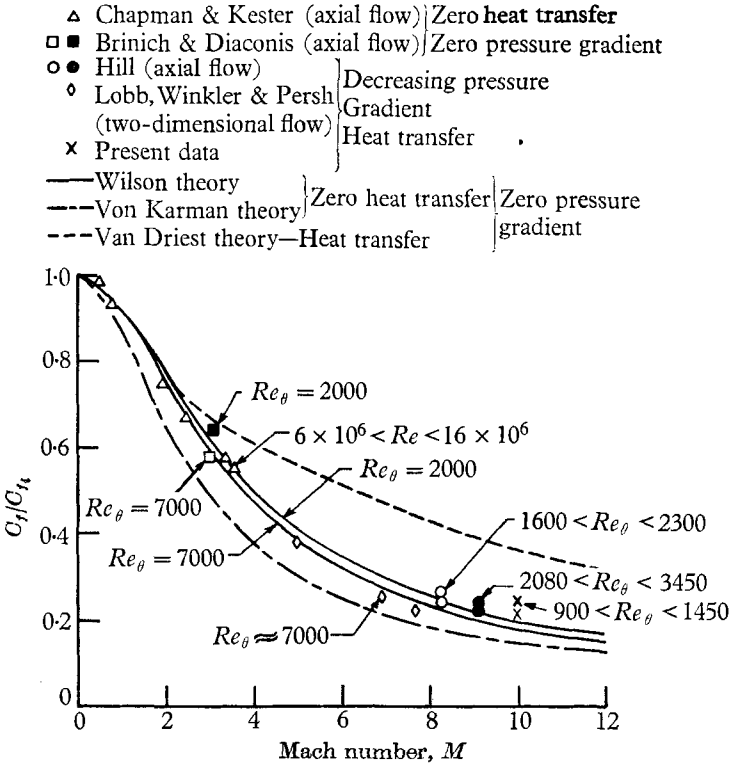

FIGURE 20. Turbulent skin-friction ratio *vs* free-stream Mach number.

number location could have been used with identical arguments. Using the preceding discussion for the other five heat-gauge locations, the transition Reynolds numbers were determined for the corresponding Mach numbers. The results of this investigation are shown in figure 21, where the Reynolds numbers for the beginning and end of transition are plotted versus free-stream Mach number. The data of Klebanoff, Tidstrom & Sargent; Potter & Whitfield; Coles; and Korkegi (1956) that are presented, were obtained in continuous-flow facilities under adiabatic wall conditions as compared with the cool-wall condition for the present data. As indicated, there is a decrease in the transition Reynolds number in the supersonic range, after which it increases through the present range of data. For the smooth-tip natural transition, the Reynolds-number curve is still rising at $M = 10{\cdot}5$ for both the beginning and end of transition. The question that is left to be answered is whether or not the transition Reynolds-number curve continues to increase or reaches some asymptotic value at higher Mach numbers. Further work is presently under way at the General Electric Research Laboratory to try to answer this question.

From figure 21 it is also possible to observe graphically the strong effect of

surface roughness. The increment in Reynolds number between the beginning and end of transition is much less for the rough sharp-tip than for the smooth-tip cone. This effectively means that the surface roughness greatly shortens the transition region. The agreement of the adiabatic and cool-wall conditions at a Mach number of about 8 indicates that the wall cooling effect in stabilizing the laminar boundary layer is small at high Mach numbers.

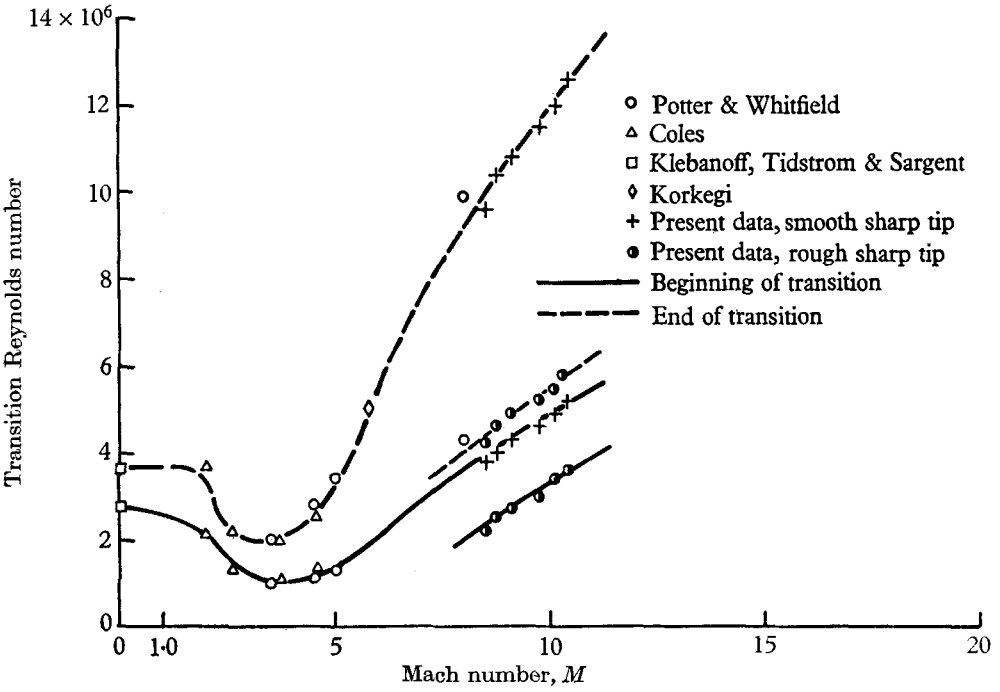

FIGURE 21. Comparison of transition Reynolds number as a function of Mach number for different flow facilities.

4.2. *Effects of tip bluntness*

With the sharp-tip data as background information it was possible to study the effects of different types of tip bluntness. As before, the discussion of the heat-transfer data will focus on the location of the first heat-transfer gauge. The various tips will be designated as shown in figure 1. The hemisphere and flat blunt tips have a diameter of 0·400 in., while the flat face of the rough blunt tip has a diameter of 0·072 in. The lowest reservoir conditions used for the study of bluntness effects were $T_5 = 1400\,°\mathrm{K}$ and $P_5 = 585$ psia (figure 6). It can be seen in this figure that the three types of bluntness—hemisphere, flat, and rough—gave the same results for laminar boundary-layer flow with no significant difference in magnitude. All the heat-transfer magnitudes for bluntness are slightly above the smooth-tip case. With these conditions the Reynolds number was too low to separate the effects of the different tips on transition.

The next higher reservoir pressure studied was $P_5 = 890$ psia (figure 8). This figure was discussed previously, and it shows the rough sharp tip to be in turbulent

flow, the smooth sharp tip to be in transition flow, and the hemisphere tip to be in laminar flow. The hemisphere tip gave a smooth heat trace which is indicative of laminar flow. From figure 8, it is evident that, with the proper tip, it is possible to either delay or promote boundary-layer transition.

In figure 9 a comparison of tip bluntness in the three different cases is made. Actually, owing to the physical size of the tip bluntness, only the hemisphere and flat blunt tip can be compared directly, while the rough blunt tip must be compared with the rough sharp tip. In figure 9 it is observed that there is no significant difference between the hemisphere and flat blunt tip since they both indicate a laminar boundary layer with nearly the same local heat-transfer magnitude. On the other hand, the rough blunt tip shows large oscillations compared with the small oscillation for the rough sharp tip with the same reservoir conditions. This would indicate the rough blunt tip to be in transition flow at the first heat-gauge location, whereas the rough sharp tip would be in fully turbulent flow. Therefore, all three types of blunt tips demonstrate that bluntness tends to delay boundary-layer transition to some degree.

The hemisphere tip was tested at higher reservoir pressures in order to obtain information regarding the incremental increase in the transition Reynolds number due to bluntness. At a reservoir pressure of 1300 psia, the hemisphere tip gave transition flow at the first heat gauge, figure 10. The hemisphere was still in transition flow at $P_5 = 2200$ psia, which was the highest reservoir pressure tested, figure 12. This is the correct trend, since it required $P_5 = 2200$ psia to put the smooth sharp-tip configuration in fully turbulent flow. The incremental increase in the critical transition Reynolds number for the hemisphere tip over that for the sharp tip is $\Delta Re_{tr} = 1{\cdot}4 \times 10^6$, which is about a 35 % increase for a cone base-diameter to tip-diameter ratio of 20. This percentage increase is in the same range as that indicated by Brinich & Sands (1957) for bluntness effects of a 10° cone on boundary-layer transition at a Mach number of 3·1.

4.3. *Effects of angle of attack*

The angle-of-attack data were obtained by pitching the model to plus and minus two degrees while holding the cone tip on the nozzle axis. Cone surface pressure and local heat-transfer data were obtained for both configurations. The pressure and heat gauges remained in the vertical plane with respect to the pitch axis. The pressure data indicated that the various configurations did not significantly affect the basic nozzle flow. It also indicated that there was no boundary-layer separation on the sheltered side of the model. Three reservoir pressures at a stagnation temperature of 1400 °K were used in this preliminary angle-of-attack study: $P_5 = 450$ psia, $P_5 = 585$ psia, and $P_5 = 1300$ psia. Only the smooth sharp tip was used, which leaves the surface roughness and bluntness effects for further study.

Typical oscilloscope traces for one heat-transfer gauge are presented in figure 4. The plus angle of attack is taken to be with the heat gauges on the sheltered side of the cone and the minus angle of attack to be with the heat gauges on the windward side. Considering the 450 psia reservoir pressure, the $\alpha = 0°$ trace is very smooth while the $\alpha = +2°$ trace shows sizeable oscillations which are

indications of transition flow. At the $P_5 = 1300$ psia condition, the $\alpha = -2°$ condition is in the early stages of transition, the $\alpha = 0°$ condition is well into transition, and the $\alpha = +2°$ condition consists of small high-frequency oscillations, which are typical of turbulent flow. From these heat-transfer traces, it is

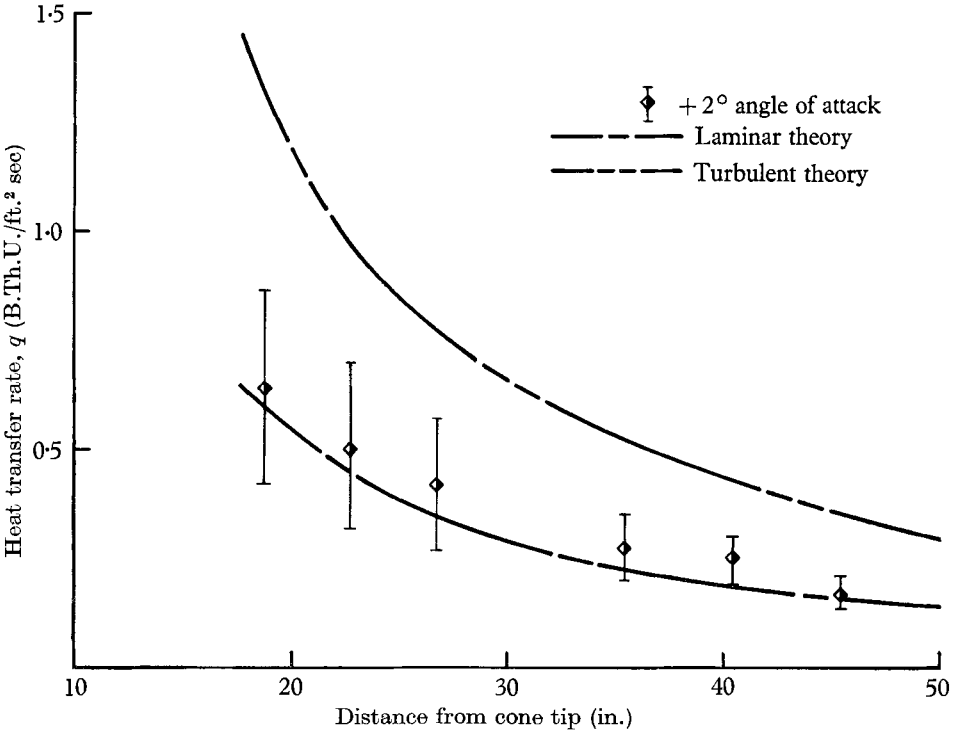

FIGURE 22. Heat-transfer distribution for smooth-tip cone at +2° angle of attack, $P_5 = 450$ psia, $T_5 = 1400$ °K.

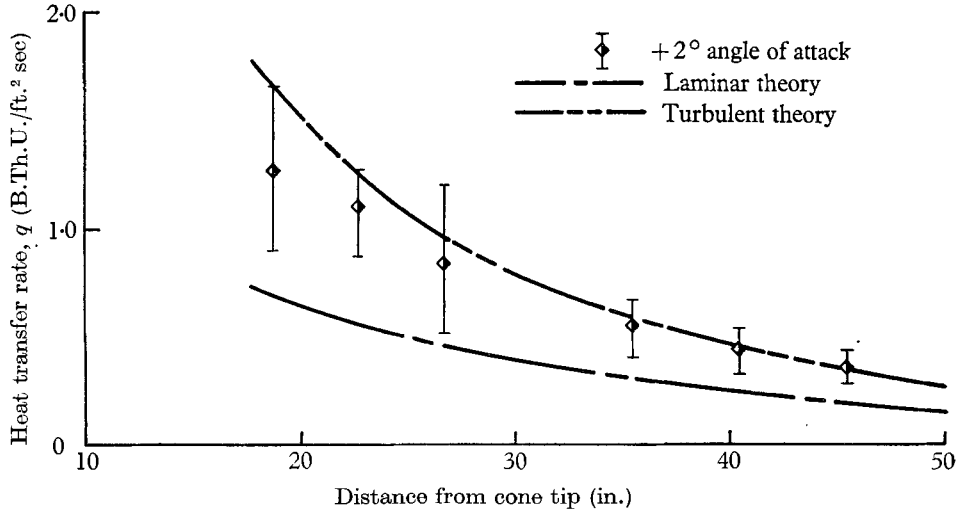

FIGURE 23. Heat-transfer distribution for smooth-tip cone at +2° angle of attack, $P_5 = 585$ psia, $T_5 = 1400$ °K.

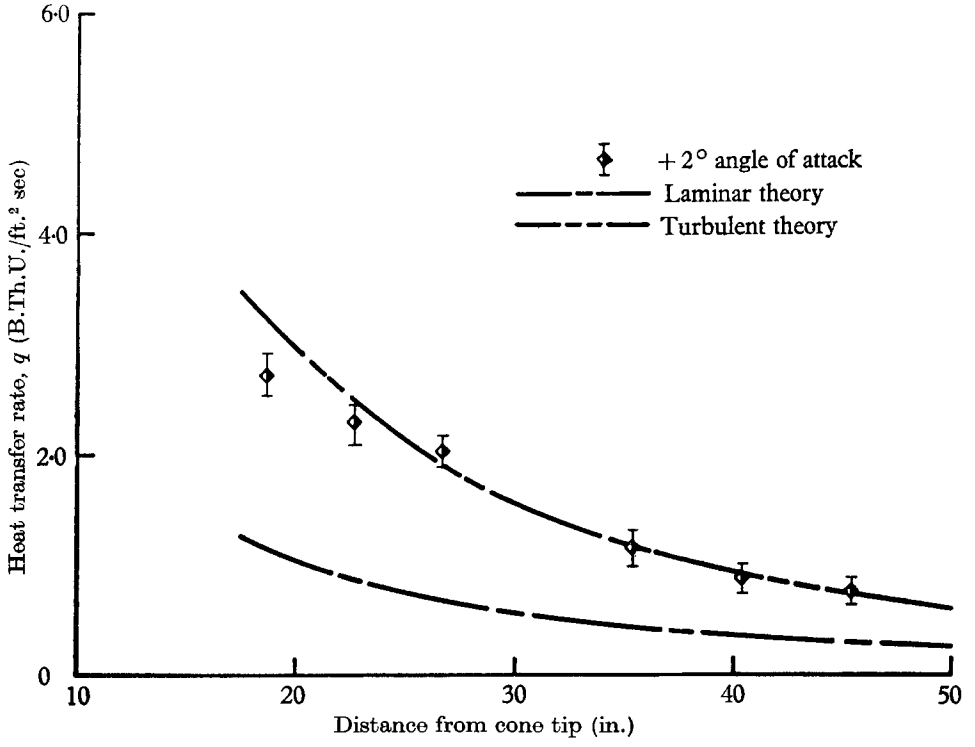

FIGURE 24. Heat-transfer distribution for smooth-tip cone at +2° angle of attack, P_5 = 1300 psia, T_5 = 1400 °K.

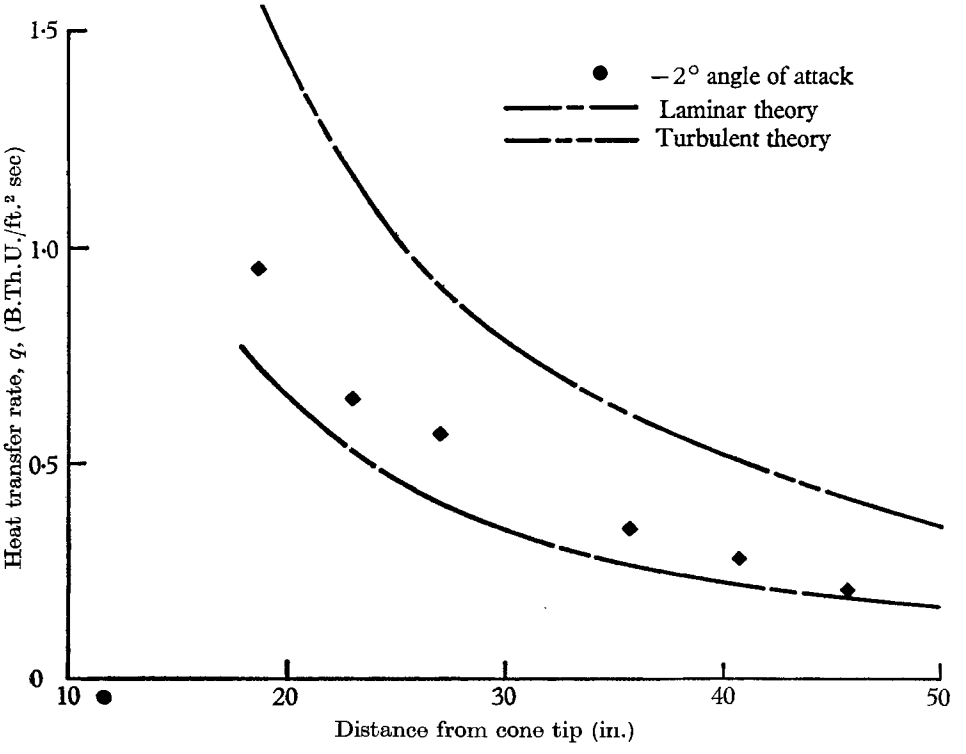

FIGURE 25. Heat-transfer distribution for smooth-tip cone at −2° angle of attack, P_5 = 450 psia, T_5 = 1400 °K.

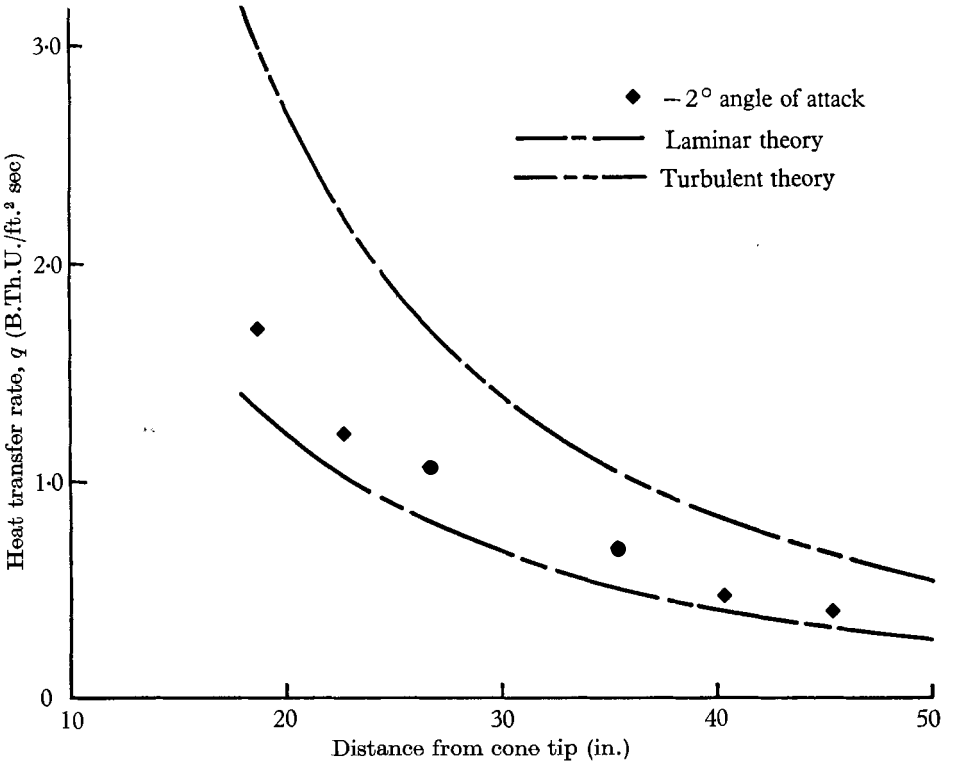

FIGURE 26. Heat-transfer distribution for smooth-tip cone at −2° angle of attack, P_5 = 585 psia, T_5 = 1400 °K.

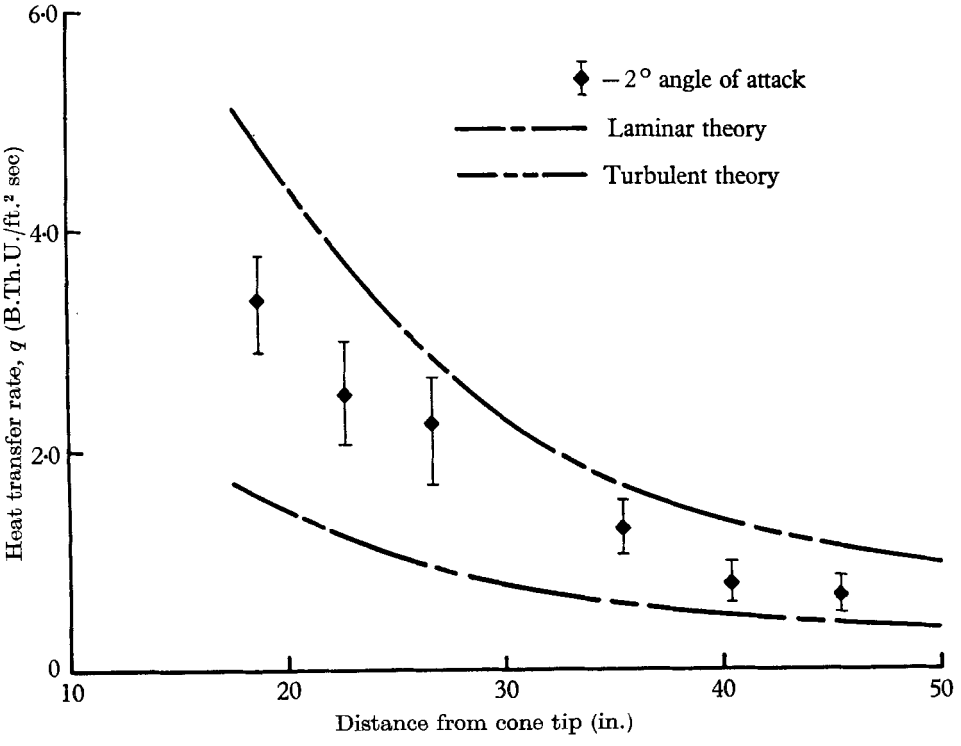

FIGURE 27. Heat-transfer distribution for smooth-tip cone at −2° angle of attack, P_5 = 1300 psia, T_5 = 1400 °K.

already evident that the cross flow, due to the angle of attack, is very effective in controlling the type of boundary layer generated.

The local heat-transfer distributions for both angles of attack are presented in figures 22 to 27. The curves in these figures were calculated using the previous zero angle-of-attack theories, the $\pm 2°$ cone surface-pressure distributions, and the work of Reshotko (1957). The first three figures in the series contain the $+2°$ results, i.e. heat gauges on the sheltered side of the cone. Focusing on the first heat-gauge location, the reservoir pressure of 450 psia (figure 22) placed this location in transition flow, where previously, at zero angle of attack, it gave smooth laminar boundary-layer flow (figure 5). The 585 psia reservoir pressure still places the first heat gauge in transition flow, but the magnitude has increased toward the turbulent theory (figure 23). The 1300 psia reservoir pressure (figure 24), shows the heat transfer to have small oscillations with the magnitude close to that of the turbulent theory; hence, the conclusion would be that turbulent boundary-layer flow exists for $+2°$ angle of attack at this pressure. The Reynolds number at this location and pressure is approximately 5×10^6. This points out that the cross flow has destabilized the laminar boundary layer to the extent of reducing the end-of-transition Reynolds number on the sheltered side of the cone by approximately 60 % of that for zero angle of attack.

The minus angle-of-attack data are presented in figures 25 to 27. From figure 25, the 450 psia reservoir-pressure condition gave smooth heat traces with no oscillations, which are characteristic of laminar flow. The deviation between the experimental data and laminar theory is about the same as for the zero-angle-of-attack case. The actual heat-transfer magnitude is greater than for the corresponding $\alpha = 0°$ due to the cross-flow effect on the windward side. The results for the 585 psia reservoir pressure (figure 26) are similar to the 450 psia pressure with the boundary layer remaining laminar. The 1300 psia reservoir condition presents a different picture in that oscillations are present in the heat gauge traces, and the heat-transfer magnitude is approaching the turbulent value. This particular situation is that of transition flow with a Reynolds number of 6×10^6 at the first heat gauge. This is a delay in the beginning of transition on the windward side with an increase in Reynolds number of approximately 60 % of that of the zero angle of attack. Thus, the windward-most boundary layer changed from laminar to transition flow as the reservoir pressure increased from 450 psia to 1300 psia.

With respect to $\alpha = 0°$, the cross flow for $\alpha = 2°$ caused the transition to move forward on the sheltered side of the cone and backward on the windward side. This result is in agreement with the free-flight data of Jedlicka, Wilkins & Seiff at a Mach number of 3·5. The significance of this result applies to the re-entry nose cone flying at varying angles of attack. As demonstrated, the cross flow at angle of attack will cause the transition point to oscillate along the body surface, which in turn will affect the body wake. Some vehicles might have a completely laminar boundary layer and wake at zero angle of attack, while at some other angle of attack the transition of the boundary layer may occur and change the wake characteristics, with a corresponding change in the ground radar image.

5. Conclusions

The laminar boundary-layer transition on a 10° cone was investigated in a shock tunnel over the Mach-number range of 8·5 to 10·5. The stagnation temperature for all the tests was approximately 1400 °K, which gave a nearly perfect-gas flow. Therefore, the Reynolds number was varied at any given cone location by simply varying the reservoir pressure.

The effects of Mach number, surface roughness, tip bluntness, and 2° angle of attack on the boundary-layer transition were investigated. Surface heat-transfer gauges were the primary instruments used to locate the beginning and end of the transition region. These gauges had a response time of a few microseconds, which enabled them to detect the turbulent bursts as they crossed the gauges. It was further demonstrated in this report that the transition of the hypersonic laminar boundary layer starts with the appearance of turbulent spots or bursts in the same manner as for subsonic transition. Schlieren photographs and a Pitot-tube boundary-layer survey were used to verify the interpretation of the local heat-transfer data. The measured cone surface-pressure data were used to check the basic nozzle flow and determine the flow properties just outside the boundary layer.

The natural boundary-layer transition for the smooth sharp tip had a long transition region with the beginning- and end-of-transition Reynolds numbers of $3{\cdot}8 \times 10^6$ and $9{\cdot}6 \times 10^6$ for the 8·5 Mach-number location. On the other hand, the beginning- and end-of-transition Reynolds numbers were $2{\cdot}2 \times 10^6$ and $4{\cdot}2 \times 10^6$ at the same location for the rough sharp tip, which demonstrates the effectiveness of proper tip surface roughness in promoting transition. Surface cooling indicated no particular stabilizing effect on the laminar boundary layer when compared with the adiabatic wall condition at hypersonic Mach numbers.

The schlieren results gave visual evidence of the start of transition, with the burst formation followed by laminar flow. They also presented turbulent flow as having a waffle-type appearance, as would be expected, since the turbulent action would tend to smooth out the steep density gradients of the hypersonic laminar boundary layer at the outer edge.

The boundary-layer Pitot-tube survey was conducted at a Mach number of 10 location. The total-pressure profiles showed a large difference between the laminar and turbulent flows. The transition flow had large oscillations, especially towards the outer edge of the boundary layer. This maximum-oscillation layer agreed with the heat-gauge results, which indicated the turbulent bursts to be moving at approximately 0·9 of the free-stream velocity. The critical layer, point of maximum oscillation, is thus well removed from the wall at the present hypersonic conditions, which would help to explain why the wall cooling effect for stabilization is small.

The velocity, temperature, and density profiles determined from the impact data were the same for both the natural and roughness-induced turbulent boundary layer, which indicates that the boundary-layer flow does not have a past history once it is turbulent. The skin-friction data obtained from the velocity profiles correlated quite well with the heat-transfer data through the modified

Reynolds analogy. The turbulent skin-friction and heat-transfer data agreed reasonably well with the corresponding flat-plate empirical theories without any transverse curvature correction, which implies that no such correction is necessary at high Mach numbers. This particular implication must be checked further experimentally for verification at high Mach numbers.

The bluntness results demonstrated that the tip bluntness delays transition over that of the sharp-tip configuration for both the smooth and rough case. There was no significant difference between the hemisphere blunt tip and flat blunt tip configuration for the reservoir conditions tested. The incremental increase in the beginning-of-transition Reynolds number due to the hemisphere was $1{\cdot}4 \times 10^6$ for a bluntness ratio of 20. Further investigations must be conducted to determine ΔRe_{tr} as a function of bluntness ratio at high Mach numbers.

The 2° angle-of-attack data pointed out the strong influence of the cross flow on the boundary layer. The end-of-transition Reynolds number decreased by 60 % on the sheltered side of the model as compared with that of the zero angle of attack, while the beginning-of-transition Reynolds number increased by 60 % on the windward side. That is, the cross flow promotes transition on the sheltered side and delays it on the windward side. Further study is necessary to determine the effects of bluntness and surface roughness, combined with angle of attack, on the transition of the hypersonic laminar boundary layer.

The support of A. J. Nerad contributed to the attainment of results presented in this paper. K. H. Cary and L. A. Osburg assisted with the instrumentation and mechanical design. This work was partially supported by the Ballistics Systems Division, United States Air Force.

REFERENCES

Brinich, P. F. & Diaconis, N. S. 1952 *Nat. Adv. Comm. Aero., Wash., Tech. Note* no. 2742.

Brinich, P. F. & Sands, N. 1957 *Nat. Adv. Comm. Aero., Wash., Tech. Note* no. 3979.

Chapman, D. R. & Kester, R. H. 1953 *J. Aero. Sci.* **20**, 441.

Coles, D. 1954 *J. Aero. Sci.* **21**, 433.

Demetriades, A. 1958 *J. Aero. Sci.* **25**, 579.

Hill, F. K. 1956 *J. Aero. Sci.* **23**, 35.

Jedlicka, J. R., Wilkins, M. E. & Seiff, A. 1954 *Nat. Adv. Comm. Aero., Wash., Tech. Note* no. 3342.

Kármán, T. von 1934 *J. Aero. Sci.* **1**, 1.

Klebanoff, P. S., Tidstrom, K. D. & Sargent, L. M. 1962 *J. Fluid Mech.* **12**, 1.

Korkegi, R. H. 1956 *J. Aero. Sci.* **23**, 97.

Laufer, J. & Verbalovich, T. 1960 *J. Fluid Mech.* **9**, 257.

Lees, L. 1947 *Nat. Adv. Comm. Aero., Wash., Tech. Rep.* no. 876.

Lees, L. & Reshotko, E. 1962 *J. Fluid Mech.* **12**, 555.

Levensteins, Z. J. 1963 *U.S. Naval Ord. Lab. Publ.*

Lin, C. C. 1955 *The Theory of Hydrodynamic Stability.* Cambridge University Press.

Little, W. J. 1963 *Arnold Eng. Dev. Ctr. Rep.* no. TDR 63-190.

Lobb, K. R., Winkler, E. M. & Persh, J. 1955 *U.S. Naval Ord. Lab. Rep.* no. 3880.

Lyons, W. C. & Sheetz, N. W. 1961 *U.S. Naval Ord. Lab. Rep.* no. 61–83.

Nagamatsu, H. T., Geiger, R. E. & Sheer, R. E. 1959 *J. ARS*, **29**, 332.

NAGAMATSU, H. T., GRABER, B. C. & SHEER, R. E. 1965 *Phys. Fluids*, **8**, 211.

NAGAMATSU, H. T. & SHEER, R. E. 1964 *Proc. AIAA Entry Technology Conf.*, p. 136, Williamsburg, Virginia.

NAGAMATSU, H. T., WEIL, J. A. & SHEER, R. E. 1962 *J. ARS*, **32**, 533.

NAGAMATSU, H. T., WORKMAN, J. B. & SHEER, R. E. 1961 *J. Aero. Sci.* **28**, 833.

PERSH, J. 1955*a* *U.S. Naval Ord. Lab. Rep.* no. 3854.

PERSH, J. 1955*b* *U.S. Naval Ord. Lab. Rep.* no. 4099.

POTTER, J. L. & WHITFIELD, J. D. 1962 *J. Fluid Mech.* **12**, 508.

RESHOTKO, E. 1957 *Nat. Adv. Comm. Aero., Wash., Tech. Note* no. 4152.

SCHLICHTING, H. 1960 *Boundary Layer Theory*. New York: McGraw-Hill.

SCHUBAUER, G. B. & KLEBANOFF, P. S. 1955 *Nat. Adv. Comm. Aero., Wash., Tech. Note* no. 3489.

SCHUBAUER, G. B. & SKRAMSTAD, H. K. 1948 *Nat. Adv. Comm. Aero., Wash., Tech. Rep.* no. 909.

TOLLMIEN, W. 1936 *Nat. Adv. Comm. Aero., Wash., Tech. Memo* (English translation) no. 792.

VAN DRIEST, E. R. 1951 *J. Aero. Sci.* **18**, 145.

WEIL, H. 1951 *J. Aero. Sci.* **18**, 311.

WILSON, R. E. 1950 *J. Aero Sci.* **17**, 585.

YOUNG, A. D. 1953 See Howarth, L., p. 402, *Modern Developments in Fluid Dynamics High Speed Flow*. Oxford University Press.